



Machine learning–assisted prediction of heat fluxes through thermally anisotropic building envelopes[☆]

Zhenglai Shen^a, Som Shrestha^{a,*}, Daniel Howard^a, Tianli Feng^b, Diana Hun^a, Buxin She^c

^a Buildings and Transportation Science Division, Oak Ridge National Laboratory, Oak Ridge, TN, 37831, USA

^b Department of Mechanical Engineering, The University of Utah, Salt Lake City, UT, 84112, USA

^c Department of Electrical Engineering and Computer Science, The University of Tennessee, Knoxville, TN, 37996, USA

ARTICLE INFO

Keywords:

Thermally anisotropic building envelope (TABE)
Machine learning
Heat flux prediction
Building energy management

ABSTRACT

Thermally anisotropic building envelope (TABE) is a novel active building envelope that can save energy use to maintain thermal comfort in buildings by redirecting heat and coolness from building envelopes to thermal loops. Finite element models (FEMs) can be used to compute the heat fluxes through TABEs, but the high computational cost of finite element simulations has prevented parametric studies and design optimizations. This paper proposes a domain knowledge–informed, finite element–based machine learning framework to reduce the computation cost for the energy management of buildings installed with TABE that uses a ground thermal loop. First, the training heat flux data set was generated by FEM simulations with different thermal loop schedules. Then, both shallow learning models (i.e., multivariate linear regression and eXtreme Gradient Boost, or XGBoost) and a deep learning model (i.e., deep neural network, or DNN) were trained to predict the heat fluxes. Domain knowledge was used for data preprocessing and feature selection. Finally, the suitability of the selected machine learning model was tested under different thermal loop schedules. The case study results showed that: (1) XGBoost can be as accurate as DNN (coefficient of determination equal to 0.81) with much less training time; (2) the annual energy cost savings for different thermal loop schedules obtained by the XGBoost-predicted and FEM-calculated heat fluxes are consistent, having a difference of only 4%; and (3) XGBoost can reduce the computation time for the annual energy analysis of the case study building with a given thermal loop schedule from around 12 h by using FEM to less than 1 min.

1. Introduction

1.1. Background

Buildings accounted for 30% of global energy use and almost 28% of total energy-related CO₂ emissions in 2019 [1]. Heating and cooling building spaces use most of this energy, accounting for approximately 42% of energy use in US residential buildings [2] and approximately 36% of energy use in US commercial buildings [3]. Building envelopes are one of the most important components that separate the indoor environment from the outdoor environment and provide residents with their desired thermal comfort. The building envelope includes the

opaque envelope, such as the exterior walls and roofs, and the transparent envelope, such as the windows. An estimated 28% of building energy use was attributed to the opaque building envelope [4]. Therefore, thermal management of the opaque building envelope is of paramount importance in reducing energy usage.

Both passive and active building envelopes have been explored in previous research to reduce unwanted heat flows passing through the envelopes. For passive building envelopes, increasing thermal resistance (*R*-value) and thermal mass are usually adopted [5,6]. The *R*-value of walls is important because it is inversely proportional to the heat flow passing through the walls. Recently, researchers have extensively studied increasing the *R*-value by adopting high-performance insulation materials, such as vacuum insulation panels and aerogels [7–9].

[☆] Notice: This manuscript has been authored by UT-Battelle, LLC, under contract DE-AC05-00OR22725 with the US Department of Energy (DOE). The US government retains and the publisher, by accepting the article for publication, acknowledges that the US government retains a nonexclusive, paid-up, irrevocable, worldwide license to publish or reproduce the published form of this manuscript, or allow others to do so, for US government purposes. DOE will provide public access to these results of federally sponsored research in accordance with the DOE Public Access Plan (<http://energy.gov/downloads/doe-public-access-plan>).

* Corresponding author. Bethel Valley Road, PO Box 2008 MS-6070, Oak Ridge, TN, 37831-6070, USA.

E-mail address: shresthass@ornl.gov (S. Shrestha).

List of abbreviations	
<i>Abbreviation Definition</i>	
Adam	Adaptive moment estimation
ANN	Artificial Neural Network
CS	Cooling season Schedule
DNN	Deep Neural Network
DOE	The US Department of Energy
EL	Exterior thermal Loop
FEM	Finite Element Model
GPM	Gallons Per Minute
GL	Ground thermal Loop
HS	Heating season Schedule
HVAC	Heating Ventilation and Air Conditioning
IL	Interior thermal Loop
MAE	Mean Absolute Error
ML	Machine Learning
MLR	Multivariate Linear Regression
MSE	Mean Squared Error
relu	rectified linear unit
RMSE	Root Mean Squared Error
RMSProp	Root Mean Squared Propagation
SGD	Stochastic Gradient Descent
TABE	Thermally Anisotropic Building Envelope
TS	Transition season Schedule
TOD	Time-Of-Day
XGBoost	eXtreme Gradient Boost

However, high cost and durability issues prevent their wide adoption in building envelopes [8–11]. Alternatively, increasing the thermal mass of building envelopes has also shown the potential to reduce heating and cooling loads and to improve indoor thermal comfort [12]. A viable way to increase the thermal mass is to incorporate phase change materials into the building envelope [13,14]. However, there is a lack of large-scale applications to show its feasibility.

Active building envelopes can be classified into four categories: air-based, water-based, solid-based, and kinetic [15]. Researchers have studied the concepts of the active air permeable wall system [16], active pipe-embedded wall system [17,18], solid-based active photovoltaic–thermoelectric wall system [19,20], and dynamic insulation system [21]. Compared with passive building envelopes, active building envelopes have an advantage owing mainly to their adaptive and tunable (controllable) attributes. Recently, researchers at the US Department of Energy’s (DOE’s) Oak Ridge National Laboratory developed a water-based active building envelope, namely the *Thermally Anisotropic Building Envelope* (TABE) [22–24] to improve thermal management in building envelopes. Fig. 1 shows the schematic of TABE connected to a ground thermal loop managed by a thermal loop schedule. TABE is constructed by alternating layers of low thermal

conductive insulation boards and high thermal conductive thin metal sheets such as aluminum. Thermal anisotropy is formed through thin metal sheets to allow heat transfer in a preferential direction. Tubes, such as Cu tubes, are built in the TABE and connected to the thin metal sheets to harvest and use low-grade thermal energy, such as ground source energy (e.g., the ground temperature at a specific depth). Interior and exterior thermal loops are built in, where the interior loop is close to the indoor wall surface and the exterior loop is close to the outdoor wall surface. Thermal loops are used to collect energy from ground energy source and then supply the energy (heating and cooling energy) to TABE. According to the functionalities of the thermal loops, they are classified as Ground thermal Loop (GL), Interior thermal Loop (IL), and Exterior thermal Loop (EL). The GL is used to collect energy from ground, which may include ground heat exchangers and ground tubes. In this study, we used an idealized GL connected to TABE. The idealized GL: (1) does not consider other systems such as the ground source heat pump; (2) ignores heat gain and loss in the loop; and (3) assumes supply water temperature to be the same as the ground temperature at 6.1 m (20 feet) depth. The IL or EL is used to describe the thermal process of supplying the collected energy to the interior tube or exterior tube of TABE for heat exchange. The IL and EL of TABE are managed by a

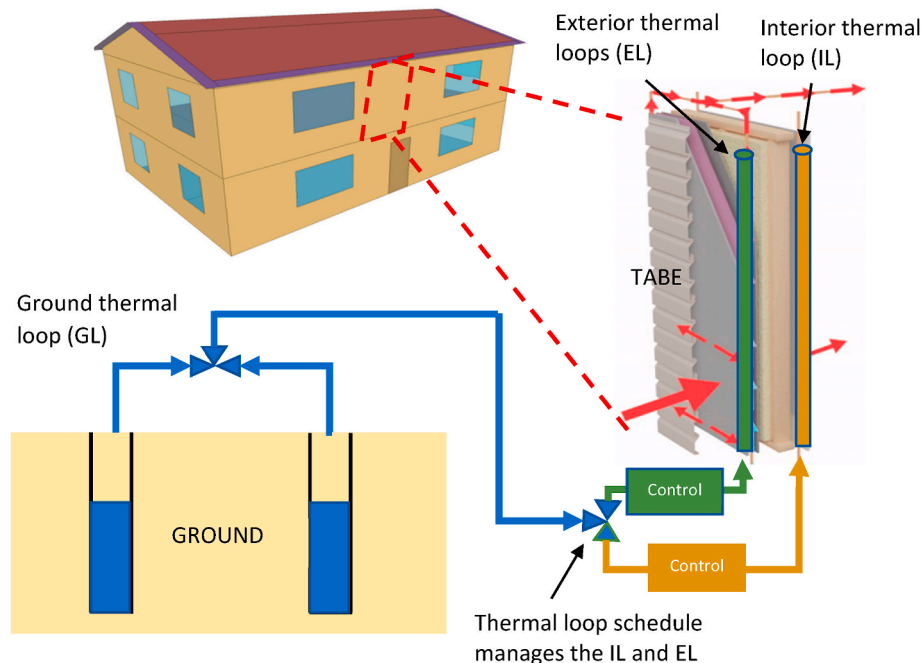


Fig. 1. Schematic of TABE with a ground thermal loop managed by a thermal loop schedule.

thermal loop schedule to achieve energy savings, where the thermal loop schedule can be constant or varied seasonally in a heating or cooling day. To avoid the potential freezing issue in cold climates, water-antifreeze solutions, such as propylene glycol at 25% weight concentration can be used as the heat transfer fluid in the EL. Laboratory and field evaluations were conducted [22,25], and the results showed that TABE was able to reduce more than 80% of the cooling load and 60% of the heating load compared with a baseline wall when circulating cold and hot water in the IL. Additionally, the Finite Element Model (FEM) of TABE was calibrated using the field evaluation data [25].

One way to evaluate the heat flow passing through the TABE is to use the physics-based model (i.e., FEM). It is comprehensive and uses physical principles to estimate the thermal dynamics and the thermal behavior of individual building components or the entire building [26]. The physics-based model involves detailed physics, which is usually called the *white-box model* and requires high expertise to develop the model and a long computation time. A given thermal loop schedule needs approximately 3 h to calculate the annual heat flux of a TABE wall. Such a long simulation time makes the determination of a suitable thermal loop schedule very challenging, especially when an optimization algorithm is needed in the process such as model predictive control. Therefore, there is a need to develop a Machine Learning (ML)-based framework to speed up the prediction of heat flux through TABE building envelopes under different operating conditions and thermal loop schedules for efficient building energy management.

1.2. Review of ML method in building energy research

ML is one of the most used data-driven methods that combines computer science and statistics, and it serves as the core of artificial intelligence and data science [27]. Unlike the physics-based model, the ML model makes a prediction without knowing the detailed physics. The ML model is also known as the *black-box model* [28]. ML has been widely used in building energy-related studies to predict a building's thermal load [29–31], energy consumption [32–34], wall heat flux [35], heat loss coefficient [36], and other related factors. Based on the model's structure, ML models can be categorized into shallow learning models and deep learning models. Shallow learning models learn from data described by predefined features and usually consist of very few layers of composition. Examples include Multivariate Linear Regression (MLR), support vector machine, decision tree, random forest, eXtreme Gradient Boost (XGBoost), and Artificial Neural Network (ANN) with one hidden layer. ANN has a strong fitting capability owing to its thousands of neurons and nonlinear activation functions, which may represent a wide variety of functions when given appropriate weights and biases [37].

Deep learning models usually have a multilayer structure, such as Deep Neural Network (DNN), or multilayer perceptron, which is an ANN model with multiple hidden layers. DNN has been proven to be adequate in approximating and solving complex problems with nonlinearities [38]. DNN has been used in building energy-related works to infer trends and generate predictions from the training data. For example, Magalhaes et al. [39] used DNN to characterize the relationship between heating energy use and heating energy demand under typical indoor and outdoor conditions in residential buildings. They concluded that DNN can be applied to estimate the heating energy use both of an individual building and at a building stock level. Ahmad et al. [40] compared the performance of a random forest and DNN to predict building energy consumption. Their results indicated that DNN performed marginally better than the random forest in predicting hourly electricity consumption. Additionally, DNN has also been applied to predict weather data [41] and solar radiation [42].

1.3. Research objectives

The first objective of this study is to address the need for an ML-based framework to predict the heat flux of TABE that uses a GL under different

thermal loop schedules to reduce the computation time. To this end, an FEM of TABE that uses a GL was established in COMSOL to calculate the hourly heat flux subject to indoor and outdoor boundary conditions that were given different thermal loop schedules and ground temperatures. The heat flux data set was then used to train the MLR, XGBoost, and DNN models. Different performance metrics were used for the model selection.

The second objective is to apply the selected trained model in a thermal loop schedule selection by comparing the energy performance of a US Department of Energy (DOE) prototype single-family residential building. The thermal loop schedules are generated by a Time-Of-Day (TOD)-based rule, which can be considered a rule-based control. The selected thermal loop schedule was compared with the baseline, whose heat flux was computed by the FEM, to test the suitability of the selected ML model.

2. Methodology

To predict the heat flux of the TABE that uses a GL for building energy management, this study proposes a domain knowledge-informed, finite element-based, data-driven framework, as shown in Fig. 2. This study consists of three main parts: (1) finite element modeling and training data set preparation, (2) domain knowledge-informed heat flux prediction, and (3) predictor-guided thermal loop schedule selection. For the finite element modeling and training data set preparation, FEM of the TABE that uses a ground thermal loop was developed for given climate conditions, ground temperatures, and thermal loop schedules. A heat flux database was established with the analysis results from the finite element analysis. The boundary conditions of the FEM were generated by the baseline EnergyPlus model, which included the factors of heat convection and thermal radiation in both the interior and exterior TABE surfaces. The generated boundary conditions of the FEM were validated by comparing the FEM-calculated heat flux with the EnergyPlus model computed counterpart for the DOE's prototype single-family residential building. For the domain knowledge-informed heat flux prediction, ML models were trained based on the established heat flux database. The models were trained with different features—the features were first selected by domain knowledge and then determined according to the correlation between each other and their importance. The domain knowledge was used to determine the potential features and their types (numerical or categorical). The performances of the models were quantified and compared by considering three performance metrics: the R^2 value, the Root Mean Squared Error (RMSE), and the Mean Absolute Error (MAE). Additionally, a ground temperature uncertainty study was conducted to understand the effects of temperature on the predicted heat flux. The purpose is to quantify the ground temperature uncertainty on the accuracy of the ML-predicted heat flux. The ground temperature is selected for uncertainty study because, physically, it will have a significant influence on the surface heat flux of TABE when the IL is activated. In the predictor-guided thermal loop schedule selection, whole-building energy analyses were conducted for a series of predicted heat fluxes on a DOE prototype single-family residential building to find the thermal loop schedule resulting in minimum annual energy cost. The heat flux was calculated by the trained ML model and the FEM with the purpose of testing the capability of the trained ML model.

2.1. Finite element modeling of TABE that uses a GL

The TABE used in this study had nominal 2×4 in. wood studs (actual measurements of 1.5×3.5 in. [3.8×8.9 cm]) at 16 in. (40.6 cm) on the center, an interior 0.5 in. (1.3 cm) gypsum board, R-13 ($13 \text{ h ft}^2 \cdot \text{°F/Btu}$ [$2.23 \text{ m}^2 \text{ K/W}$]) fiberglass bat insulation in the cavities, two layers of 0.5 in. (1.3 cm) polyisocyanurate insulation, and exterior horizontal vinyl siding, as shown in Fig. 3(a). The panel assemblies meet the International Energy Conservation Code 2018 R-value requirements for a residential building wall in ASHRAE climate zones 3 to 5. To accelerate the

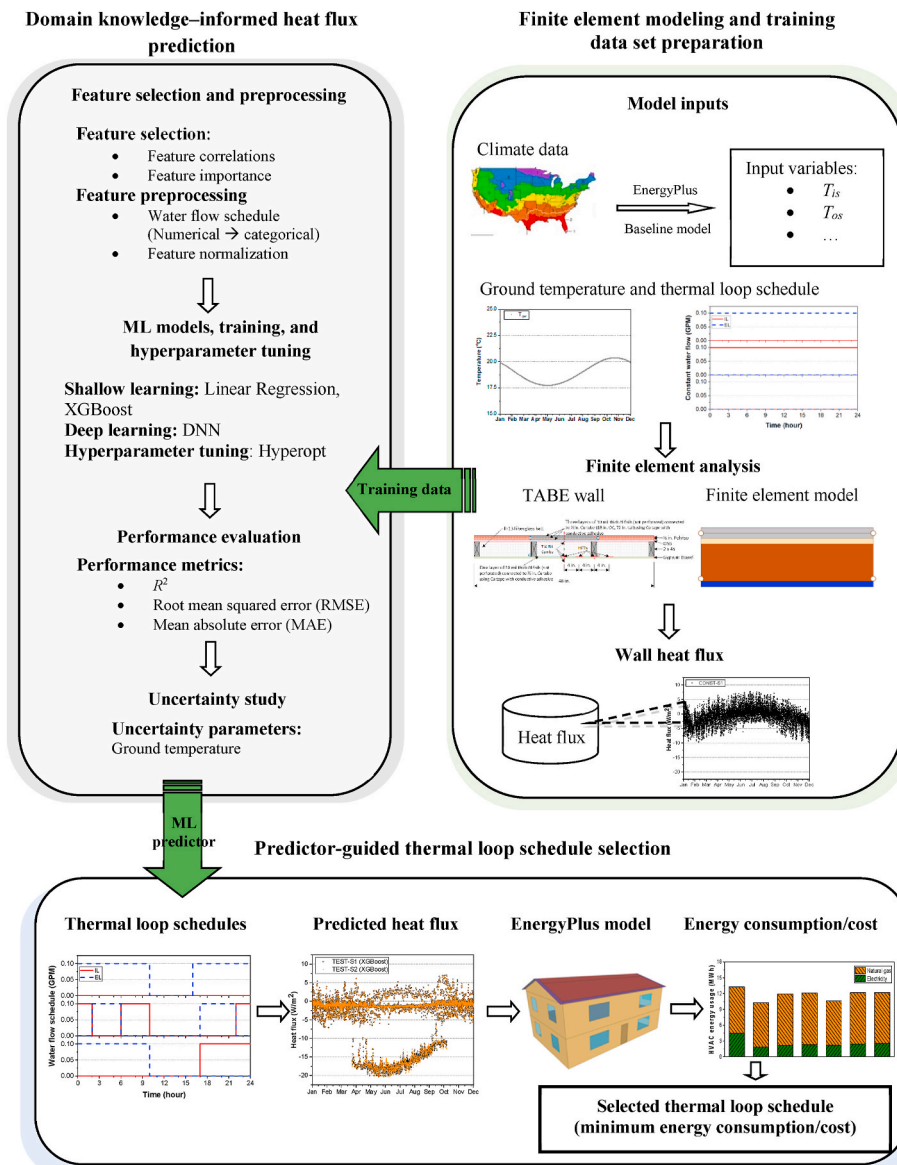


Fig. 2. A domain knowledge-informed, finite element-based ML framework for building installed TABE that uses a ground thermal loop.

heat dissipation rates, interior and exterior thermal loops were integrated into the TABE. When connecting to a GL, the TABE panel could be used as (1) an active protection to separate the indoor environment from the outdoor environment when activating the exterior thermal loop or (2) a heating and cooling source when activating the interior thermal loop with a suitable ground temperature.

A COMSOL FEM, which is shown in Fig. 3(b), was established to simulate the heat flux and thermal performance of TABE panels. The output data of COMSOL, the heat fluxes, were then used as the inputs to (1) train the ML models and (2) compute the whole-building energy consumption in EnergyPlus. The input and output variables of the FEM are listed in Table 1. The variables include 10 input variables and 1 output for each wall (4 walls for the DOE’s prototype single-family residential building that was studied). A span between adjacent thermal loop tubes with a representative area (10.76 ft² [1 m²]) of TABE was simulated for each wall. The area was subsequently scaled up to the entire opaque wall area of the prototype building. The wall surface temperature, air temperature, and radiation heat flux input data were obtained from a baseline EnergyPlus model that had a construction identical to the TABE but without metal layers and thermal loops. The ground temperature was calculated by using the method developed by

Xing et al. [43] at the depth of 6.1 m (20 ft). The ground temperature at this depth varies annual, which is relatively cold at summer time due to the phase lag effect of ground heat transfer [43].

2.2. ML algorithms

ML is a computation process used to discover patterns from data and is usually applied to model complex system behaviors or increase the computational efficiency. For TABE using a GL, the dynamic behavior is mainly due to the thermal loop schedule, creating the need to use an FEM to compute the wall heat flux, which is time consuming. ML could be a possible solution to reduce the computation time while maintaining good accuracy to differentiate thermal loop schedules. MLR, XGBoost, and DNN are adopted in this study for the following reasons: (1) MLR is the simplest shallow learning model that can be used to find a possible linear relationship between the responsive variable and the selected features, (2) XGBoost [44] is a shallow learning model developed recently with a strong fitting capability and is time efficient in training, and (3) DNN [45] performs very well with respect to complex systems but is relatively time-consuming to train.

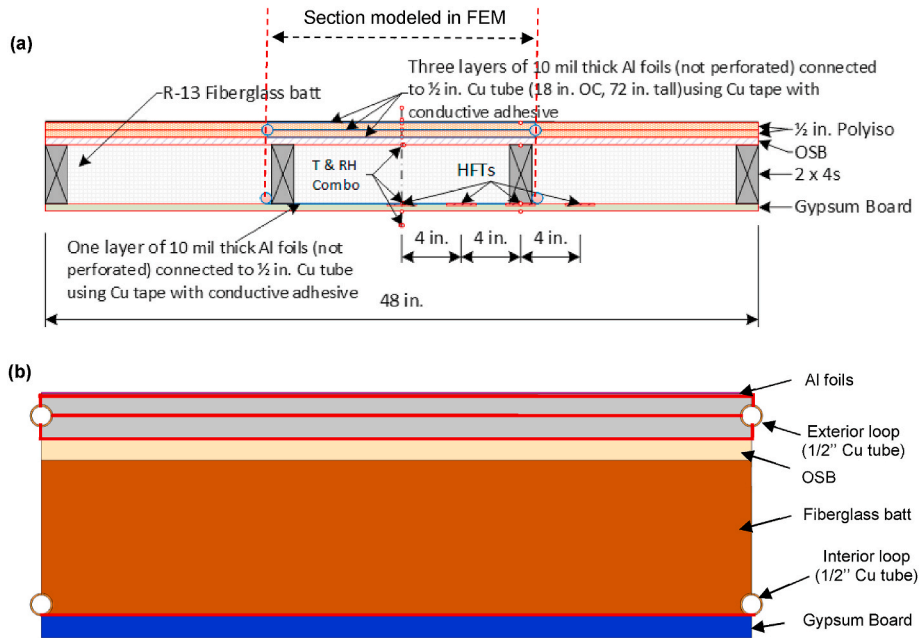


Fig. 3. Prototype TABE wall panel and finite element model: (a) schematic of a prototype TABE panel with both interior and exterior thermal loops and (b) the established finite element model in COMSOL.

Table 1
Input and output variables of FEM.

Input and output	Variables
Input	(1) Indoor wall surface temperature (T_{is}) (2) Outdoor wall surface temperature (T_{os}) (3) Indoor wall surface convection coefficient (h_i) (4) Outdoor wall surface convection coefficient (h_o) (5) Indoor air temperature (T_{ia}) (6) Outdoor air temperature (T_{oa}) (7) Indoor surface radiation ($q_{r, is}$) (8) Outdoor surface radiation ($q_{r, os}$) (9) Ground temperature (T_{gw}) (10) Thermal loop schedule (TLS)
Output	(1) Heat flux from the walls to the conditioned space (q_{is})

2.2.1. MLR

MLR is the simplest shallow learning model that can be treated as a perceptron, as shown in Fig. 4. Let (x_i, y_i) be a training instance where x_i is the features (independent variables), and y_i is the target variable (response variable). For MLR, the target variable is related to the features through Eq. (1) [46]:

$$\hat{y} = f\left(\sum_{i=1}^n w_i x_i + b\right), \tag{1}$$

where \hat{y} is the predicted target variable (heat flux), $W = (w_1, w_2, \dots, w_n)$ is

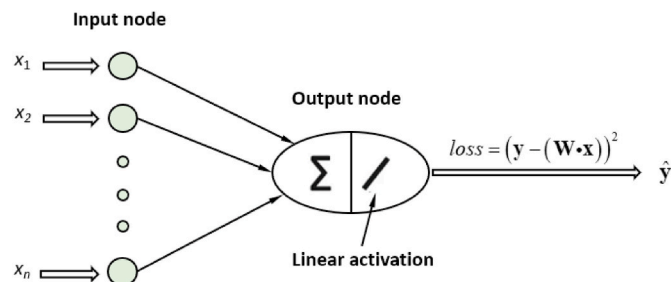


Fig. 4. Diagram of MLR structure.

an n -dimensional coefficient vector, and b is the bias that needs to be learned to minimize the total squared error on the training data (i.e., $\sum_{i=1}^n e_i^2$ with $e_i = y_i - \hat{y}_i$), $f(\bullet)$ is the activation function, which is a linear function for MLR.

2.2.2. DNN

DNN is a type of ANN with multilayer perceptron [46] inspired by the networks of biological neurons found in the human brain and is intended to mimic the brain’s behavior, allowing computer programs to recognize patterns and solve problems. DNN comprises one input layer, one or more hidden layers, and one output layer. Fig. 5 shows the structure of a DNN with two hidden layers, formulated as Eq. (2) [45]:

$$\begin{cases} y_j = f\left(\sum_{i=1}^n w_{ij} x_i + b_j\right) \\ y_k = f\left(\sum_{j=1}^{m_1} w_{jk} y_j + b_k\right) \\ \hat{y} = f\left(\sum_{k=1}^{m_2} w_{kp} y_k + b_p\right) \end{cases}, \tag{2}$$

where y_j and y_k are the outputs of hidden layer 1 (H_1) and hidden layer 2 (H_2); w_{ij} , w_{jk} , and w_{kl} are the weights connecting the input layer, H_1 , H_2 , and the output layer; b_j , b_k , and b_l are the biases; and m_1 and m_2 are the total nodes of H_1 and H_2 . The activation function in Eq. (2) is not a linear function, which can be a rectified linear unit (relu) function, sigmoid function, and hyperbolic tangent function [46].

2.2.3. XGBoost

XGBoost is a decision tree–based ensemble ML algorithm that uses a gradient boosting learning framework, as shown in Fig. 6. XGBoost was developed by Chen and Guestrin [44] and showed great success in recent ML competitions. XGBoost sequentially adds decision tree models to predict the errors of the predictor before it. XGBoost was mathematically formulated as Eq. (3) [44]:

$$L^{(l)} = \sum_{i=1}^N l\left(y_i, \left(\hat{y}_i^{(l-1)} + f_i(\mathbf{x}_i)\right)\right) + \Omega(f_i), \tag{3}$$

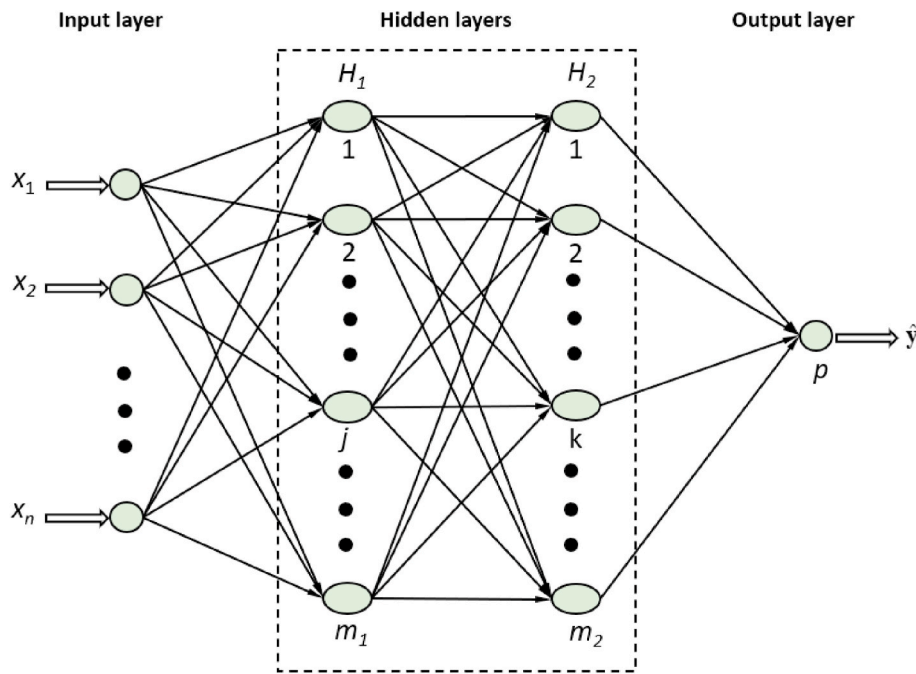


Fig. 5. Diagram of DNN structure.

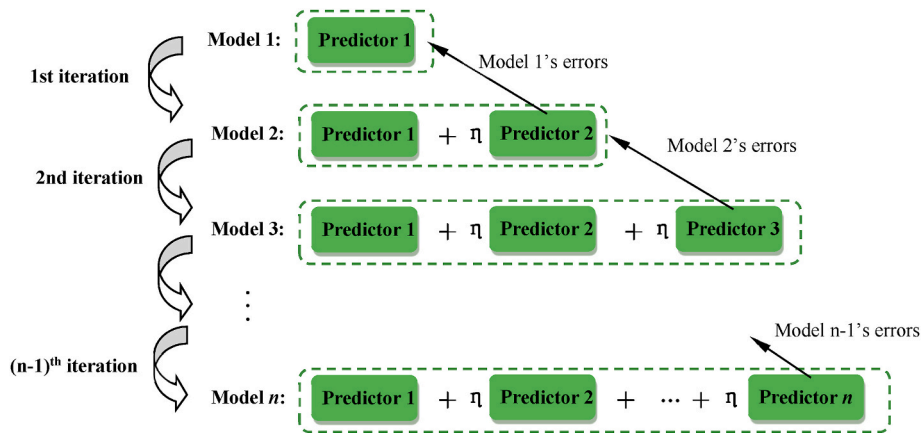


Fig. 6. Diagram of gradient boosting structure.

where I is the I th sample to be predicted, N is the total number of samples, t represents the t th iteration, $l(y_I, \hat{y}_I)$ is the loss function between the true label y_I and the predicted label \hat{y}_I , $f_t(x_I)$ is the base learner (decision tree for XGBoost) added at the t th iteration, x_I is the features of the I th sample, and $\Omega(f_t)$ is the regularization term to avoid overfitting.

2.3. Hyperparameter tuning and performance metrics

2.3.1. Hyperparameter tuning

Hyperparameter tuning is the process of searching for the most suitable hyperparameters for a ML model to a specific data set. This study used the Bayesian optimization function provided by Hyperopt [47], which is suitable for hyperparameter tuning because it is a sequential design strategy for global optimization and does not assume any functional forms. For XGBoost, a total of eight parameters were tuned, as shown in Table 2. The XGBoost algorithm has many hyperparameters that can be tuned. For a detailed description of the hyperparameters, refer to the open-source XGBoost Python package. For DNN, the batch size, number of hidden layers, and optimizer were tuned as

well as the number of neurons, learning rate, and dropout rate of each hidden layer, as shown in Table 3. The determination for the searched range of hyperparameters in XGBoost and DNN considered both their importance and typical ranges used in references and Kaggle community.¹ Meanwhile, we have used a relatively wide search range to leverage the capacity of HyperOpt. For example, 250 has been used as the maximum number of estimators for searching in XGBoost in Ref. [30] while this study used 500. In addition, the search ranges of the DNN hyperparameters are also considered for both training efficiency and accuracy. For example, the selection of the hidden layers in DNN is mainly considered in terms of training efficiency, and usually, 2–3 hidden layers can meet the training accuracy requirement. On the other hand, a common practice in setting the number of neurons in each layer is to let it be 2^n due to the binary property of the computer. In this study, we used a typical search range of 64 to 1024 neurons. After finding the best hyperparameters with Bayesian optimization, the model was

¹ See <https://www.kaggle.com>. This is a very popular and famous machine-learning community.

Table 2
Hyperparameters tuned for XGBoost.

Hyperparameters	Description	Searched range	Selected
$n_{estimators}$	Number of estimators	[100, 500, 10]	240
max_depth	The maximum depth of tree	[5, 20, 1]	19
$learning_rate$	Step size shrinkage used in update to prevent overfitting	[0.01, 0.1, 0.01]	0.02
$gamma$	Minimum loss reduction required to make a further partition on a leaf node of the tree	[0.02, 0.3, 0.02]	0.06
min_child_weight	Minimum sum of instance weight (hessian) needed in a child	[1, 6, 1]	5
$subsample$	Subsample ratio of the training instances	[0.2, 1, 0.1]	0.7
$colsample_bytree$	Subsample ratio of columns when constructing each tree	[0.5, 1, 0.1]	0.8
reg_lambda	L2 regularization ^a term on weights	[0.1, 1, 0.1]	0.3
$f(\cdot)$	Activation function	–	relu
k	Number of epochs	–	200
$loss$	Loss function	–	MSE
opt	Optimizer	–	SGD

^a L2 regularization: adding penalty for residual leaves by using ridge regularization (L2).

Table 3
Hyperparameters tuned for DNN.

Layer	Hyperparameters	Description	Searched range	Selected
1	$n^{[l]}$	Number of neurons	[64, 1024, 64]	768
	lr	Learning rate	[0.005, 0.1, 0.005]	0.02
	dp	Dropout	[0.25, 0.75, 0.25]	0.5
2	$n^{[l]}$	Number of neurons	[64, 1024, 64]	640
	lr	Learning rate	[0.005, 0.1, 0.005]	0.025
	dp	Dropout rate	[0.25, 0.75, 0.25]	0.25
	bs	Batch size	[32, 256, 16]	48
	$n^{[h]}$	Number of hidden layers	[2, 3, 1]	2
	$f(\cdot)$	Activation function	–	relu
	k	Number of epochs	–	200
	$loss$	Loss function	–	MSE
	opt	Optimizer	Adam, SGD, RMSprop	SGD

trained with the training and validation data sets and finally applied to the test data sets for the TABE wall heat flux prediction with different thermal loop schedules for building energy management. The training, validation, and test data sets are detailed in Section 3.2.1.

2.3.2. Performance metrics

The performance of regression models can be assessed through multiple metrics. In this study, the prediction performances were evaluated using three metrics: the coefficient of determination (R^2), the root mean square error (RMSE), and the mean absolute deviation (MAD), as shown in Eqs. (4)–(6), respectively.

$$R^2 = 1 - \frac{\sum_{i=1}^N (y_i - \hat{y}_i)^2}{\sum_{i=1}^N (y_i - \bar{y})^2}, \quad (4)$$

$$RMSE = \sqrt{\frac{1}{N} \times \sum_{i=1}^N (y_i - \hat{y}_i)^2}, \quad (5)$$

$$MAD = \frac{1}{N} \times \sum_{i=1}^N |y_i - \hat{y}_i|, \quad (6)$$

where N is the number of observations, y_i is the i th observed value calculated by FEM; \bar{y} is the mean of the observed values, and \hat{y}_i is the i th estimated value predicted by the ML models. The prediction accuracy increased as the errors of the RMSE and MAD decreased and the R^2 increased. Both RMSE and MAD were used because (1) the RMSE is more appropriate than the MAE when the model errors follow a normal distribution and (2) the MAE is more suitable than the RMSE when outliers are present in the model [48].

2.4. Predictor-guided thermal loop schedule selection

The predictor was used to predict the heat flux of the TABE with different thermal loop schedules. For each thermal loop schedule, the heat flux of the TABE for a DOE prototype building could be predicted with the trained ML model (predictor). After that, the predicted heat fluxes were entered into the EnergyPlus model of the prototype building to calculate the annual energy consumption and costs. The annual energy consumption and costs for different thermal loop schedules were expected to be different. In this study, the thermal loop schedule that led to the minimum annual energy cost was selected. Assuming a total of n_s thermal loop schedules, the selected (or optimum) thermal loop schedule, $TLS_{selected}$, can be formulated as Eq. (7):

$$TLS_{selected} = \min\{g(TLS_1), g(TLS_2), \dots, g(TLS_{n_s})\}, \quad (7)$$

where $g(\bullet)$ is used to represent the complex relationship between the annual energy cost and the thermal loop schedule. The function considers the contributions from the ML predictor and the EnergyPlus model.

3. Case study

3.1. Climate condition and prototype building

Charleston, South Carolina, USA, was selected as the location for the case study. It has a humid subtropical climate with mild winters; hot, humid summers; and significant rainfall all year. It has a cold winter (minimum outdoor air temperature -5.6°C) and hot summer (maximum outdoor air temperature 37.8°C) with suitable ground temperatures at the depth of 6.1 m (average annual ground temperature around 19°C).

The DOE prototype single-family residential building [49] was used as the prototype building to test the proposed framework for predicting wall heat flux for building energy management. The prototype building is a two-story, south-facing building with a basement and a total floor area of 445 m^2 (see Fig. 1). The model settings and schedules, such as occupancy, lighting, equipment, ventilation, and heating and cooling, were adopted from the prototype building and can be found in Ref. [49]. The Heating Ventilation and Air Conditioning (HVAC) system used an electric variable air volume reheat system for cooling and natural gas for heating. The set points for heating and cooling were 22.2°C and 23.9°C , respectively. The characteristics of the envelope and HVAC are summarized in Table 4.

3.2. Data preparation and feather selection

3.2.1. Data preparation

The training, validation, and test data were generated by the FEM (see Fig. 3) with different thermal loop schedules. The thermal loop schedules were classified into training schedules, validation schedules, and test schedules, which are summarized in Table 5. Three constant thermal loop schedules (CONST-S1, CONST-S2, and CONST-S3) were used as the training schedules to learn the potential nonlinear dynamics.

Table 4
Summary of the characteristics of the envelope and HVAC.

Category	Item	Summary
Envelope	Roof	Area: 116.4 m ² , R-value: 4.61 m ² K/W, solar reflectance: 0.25, thermal absorptance: 0.90
	Walls	Area: 179.6 m ² , R-value: 3.17 m ² K/W, solar reflectance: 0.50, thermal absorptance: 0.88
	Window	Window to wall ratio: 0.184, U-value: 3.69 W/m ² ·K, solar heat gain coefficient: 0.334
HVAC	Heating facility	Burner efficiency: 0.80
	Cooling facility	Coefficient of performance: 4.07
	Set points	Heating: 22.2°C, cooling: 23.9°C

Table 5
Thermal loop schedules.

Category	Schedule name	Description
Training	CONST-S1	EL = 0 GPM, IL = 0 GPM
	CONST-S2	EL = 0.1 GPM, IL = 0 GPM
	CONST-S3	EL = 0 GPM, IL = 0.1 GPM
Validation	OPT	Generated by selecting the thermal loop schedule that minimized the hourly energy consumption from the schedules of CONST-S1, CONST-S2, and CONST-S3.
Test Schedules 1 (Uncertainty analysis)	TEST-S1	HS1 + TS + CS1 + T_g
	TEST-S2	HS1 + TS + CS1 + T_g with uncertainty ($T_{g,uncertainty}$)
Test Schedules 2 (Energy analysis)	TEST-S1	HS1 + TS + CS1
	TEST-S3	HS2 + TS + CS2
	TEST-S4	HS3 + TS + CS3

Then, an optimum schedule (OPT) was selected and used as the validation schedule to validate the model training. The OPT was generated by selecting the thermal loop schedules that minimized the hourly energy cost obtained from the schedules of CONST-S1, CONST-S2, and

CONST-S3, which include a variety of thermal loop schedule dynamics. Lastly, two test schedules (i.e., Test Schedule 1 and Test Schedule 2) were used to test the trained ML models.

The test schedules were composed of different combinations of the Heating season Schedule (HS), Cooling season Schedule (CS), and Transient season Schedule (TS), where TS is the same for all the test schedules. HS, CS, and TS were designed according to the time of days (TODs) and are presented in Fig. 7 (a)–(c). During the heating season (November–March), isolating the indoor environment from the cold outdoor environment is desired during the morning and night hours (TODs 0:00–10:00 a.m. and 16:00/17:00–24:00 p.m.) by turning on the EL. Meanwhile, using the relatively high ground temperature to heat the indoor environment could also provide heat during the morning and night hours by turning on the IL. On the other hand, heating requirements during the peak time hours (TODs 11:00 a.m.–16:00/17:00 p.m.) are not high owing to the outdoor solar radiation and the thermal loops can be turned off. Therefore, three different heat season schedules, HS1–HS3, were designed to reflect such a TOD regulation, as shown in Fig. 7(a).

During the cooling seasons (May–September), the cooling requirements for the morning and night hours (TODs: 0:00–6:00/8:00/9:00 a.m. and 17:00/19:00–24:00 p.m.) are not high; therefore, one can either turn on the EL or turn off the thermal loops. Alternatively, the peak hours (TODs: 6:00/8:00/9:00 a.m.–17:00/19:00 p.m.) have a high cooling requirement, and the interior thermal loop could be turned on to use the cooling energy of the ground. Similar to the heating season, three different cooling season schedules, CS1–CS3, were designed, as shown in Fig. 7(b).

The transition seasons (April and October) are characterized by relatively low heating requirements during the morning and night times (TODs 0:00–8:00 a.m. and 18:00–24:00 p.m.) and the cooling requirements during the peak hours (11:00 a.m.–15:00 p.m.), as shown in Fig. 7(c). Therefore, the EL is turned on during the morning and night times, while the IL is turned on during the peak hours. For the remaining hours of a day, the thermal loops are turned off.

Test Schedule 1 (Table 5) was used to analyze the uncertainty of ground temperature. It included TEST-S1 and TEST-S2, which are

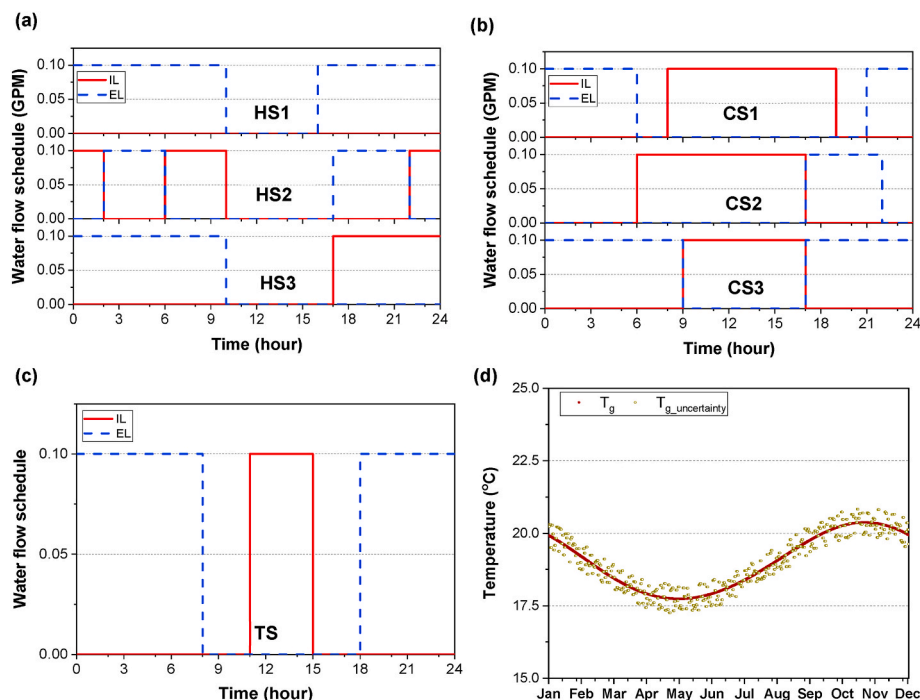


Fig. 7. Thermal loop schedules in different seasons—(a) heating season schedules (November–March), (b) cooling season schedules (May–September), and (c) transition season schedule (April and October)—and (d) ground temperature.

composed of HS1 and CS1 both considering and not considering uncertainty in ground temperature (details illustrated in Section 3.2.2). Test Schedule 2 (Table 5) included three thermal loop schedules, TEST-S1, TEST-S3, and TEST-S4, designed for the energy analysis to discover (1) the accuracy of the trained ML models in predicting heat flux and (2) the energy consumption behavior of the prototype building under predicted heat flux and heat flux calculated by FEM. The designed test thermal loop schedules were based on the authors' expertise, which did not necessarily lead to significant savings in energy consumption or cost. Additionally, the water flow rate for all the thermal loop schedules was set to 0.1 Gallons Per Minute (GPM) because preliminary studies showed that it is a relatively economical flow rate.

The heat flux calculated by the FEM for different thermal loop schedules of the TABE south wall are shown in Fig. 8. When no water flow occurred (CONST-S1), the calculation simplified into a plain wall with a specific R -value, and the climate conditions dominated the heat flux behavior. It reflected as the heat losses through the wall during heating season (negative heat flux), and heat flow passed through the wall during the cooling season (positive heat flux), as shown in Fig. 8(a). When a constant thermal loop schedule or constant water flow was applied to the exterior thermal loop (CONST-S2), the thermal loop acted as a separator that isolated the indoor environment from the outdoor environment, and the TABE heat flux only slightly varied, as shown in Fig. 8(b). The heat flux was negative for most of the experiment's duration because the ground temperature was lower than the indoor air temperature. When a constant thermal loop schedule was applied to the interior thermal loop (CONST-S3), the thermal loop acted as a cooling source constantly extracting heat from the indoor environment, as shown in Fig. 8(c). The seasonal variation of the cooling heat flux is mainly attributed to the annual ground temperature variation, as shown in Fig. 7(d). In Fig. 7(e), the uncertainty of a $\pm 0.5^\circ\text{C}$ random uniform distribution was added to the ground temperature to study its effects on

the predicted heat flux. When the thermal loop schedule was not constant, the heat flux was considered to be a combination of constant thermal loop schedules, as shown in Fig. 8(d), (e), and (f).

3.2.2. Domain knowledge-informed feature selection

Feature selection is the process of obtaining a subset of an original feature set according to certain feature selection criteria [50]. In this study, the ten input variables of FEM were considered the original feature set. Fig. 9(a) presents the feature correlation map (Pearson's correlation coefficients) for the nine variables except the thermal loop schedule. The thermal loop schedule was also selected as a training feature but was not included in the correlation study because the thermal loop schedule needed to be treated as a categorical variable instead of a numerical variable. Additionally, a feature importance study was conducted based on the XGBoost regression. The results, shown in Fig. 9(b), suggested that the interior surface temperature (T_{is}) and interior surface radiation heat flux ($q_{r,is}$) are the most important features, and the outdoor air temperature (T_{oa}) and indoor air temperature (T_{ia}) are the least important features. The F-score of the XGBoost regression measures how many times each feature was split. The features were normalized before being used to train the ML models.

The feature correlation map (Fig. 9 (a)) shows that the original features were generally not correlated with each other and were used as the features in training the ML models. The features before normalization are shown in Fig. 10. The features on the indoor side usually had a small variation compared with their counterparts on the outdoor side. The indoor and outdoor surface radiations were directed onto the surface. As mentioned in this study, radiations were extracted from the baseline EnergyPlus model. The remaining two features, i.e., thermal loop schedules and ground temperature, are shown in Fig. 7. The thermal loop schedule feature was transformed into a categorical feature by using OneHotEncoder in scikit-learn [51]. Putting domain knowledge in the features selection was critical because (1) the original features came from the FEM, which represented domain knowledge, and (2) the thermal loop schedule was treated as a categorical variable to differentiate the interior, exterior, and no water flow of TABE.

3.3. Heat flux prediction and predictor-guided thermal loop schedule selection

3.3.1. Heat flux prediction

The ML models were trained using the three constant thermal loop schedules (training data set) and the optimum thermal loop schedule for validation (validation data set), as shown in Table 5. The training data set was first shuffled to ensure its randomness. Then, 80% of the data was used for training and validation while the remaining 20% was used for testing. It is noted that the validation data set is not shuffled to ensure the training process can learn the heat flux dynamics of TABE in the OPT schedule. After training the ML models, the performance metrics (i.e., R^2 , RMSE, and MAE) were obtained and are shown in Table 6. The MLR model had a relatively poor performance with the R^2 less than 0.8. The XGBoost and DNN predictions had an R^2 larger than 0.8 for the test thermal loop schedules (i.e., TEST-S1–TEST-S4), indicating that XGBoost and DNN have the potential to be used for thermal loop schedule selection. DNN predictions have a slightly smaller RMSE but a slightly larger MAE, compared to XGBoost predictions. The predicted heat flux was further compared to determine which ML model is best to be used for the predictor-guided thermal loop schedule selection.

Fig. 11 compares the heat flux predicted by the ML models for a typical week in the heating season, transition season, and cooling season for the south wall. The heat flux predicted by the MLR model differs largely when compared with its counterparts calculated by the FEM, as indicated by the performance metrics shown in Table 6. The heat flux predicted by the XGBoost and DNN models was close to the FEM calculations. They also behaved similarly, although small differences were observed between them. For example, the heat flux predicted by the

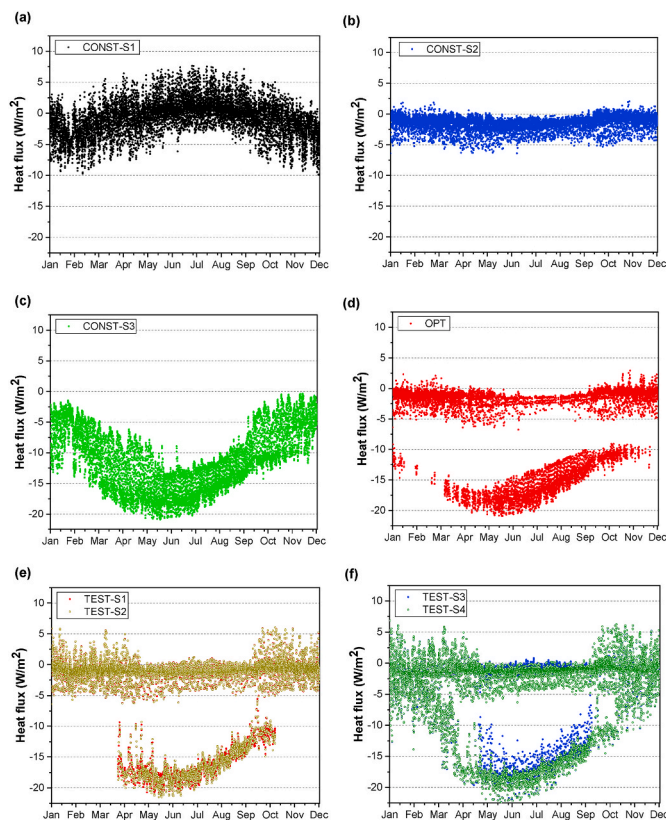


Fig. 8. TABE south wall heat flux generated by the training, validation, and test thermal loop schedules: (a) CONST-S1, (b) CONST-S2, (c) CONST-S3, (d) OPT, (e) TEST-S1 and TEST-S2, and (f) TEST-S3 and TEST-S4.

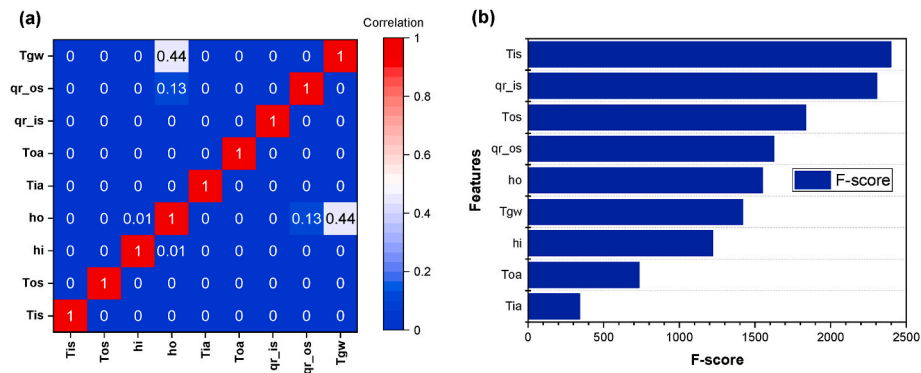


Fig. 9. Feature relationships: (a) feature correlation map and (b) feature importance.

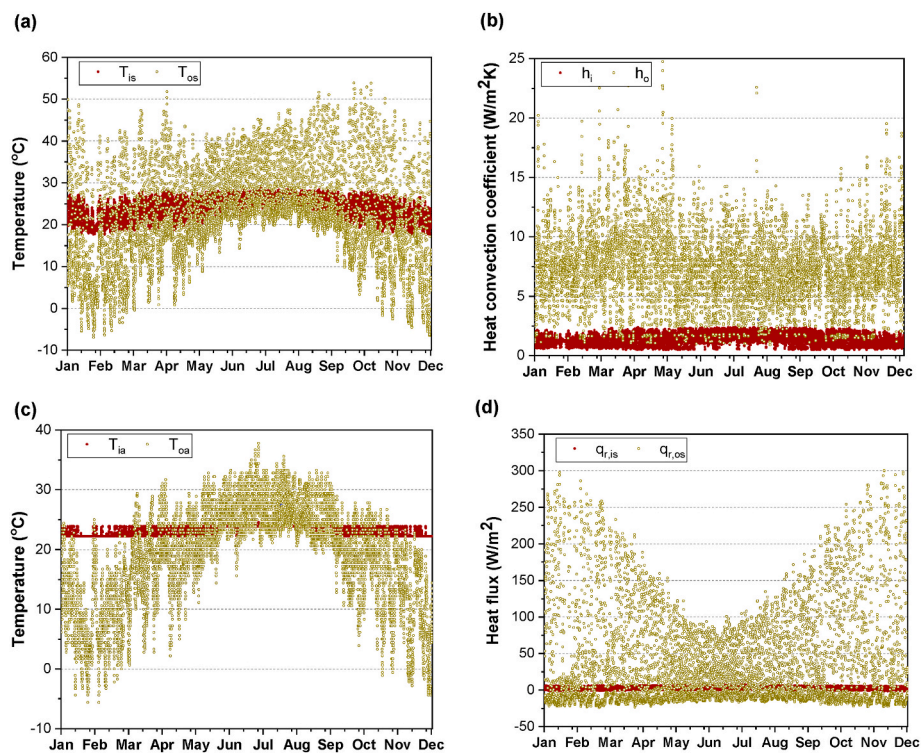


Fig. 10. ML training features: (a) indoor and outdoor surface temperatures (T_{is} and T_{os}), (b) indoor and outdoor surface heat convection coefficient (h_i and h_o), (c) indoor and outdoor air temperature (T_{ia} and T_{oa}), and (d) indoor and outdoor surface radiation heat flux ($q_{r,is}$ and $q_{r,os}$).

Table 6

Performance metrics of the training, validation, and test data sets.

Metrics	Models	Training	Validation	TEST-S1	TEST-S2	TEST-S3	TEST-S4
R^2	MLR	0.74	0.76	0.77	0.77	0.62	0.70
	XGBoost	1.00	0.91	0.81	0.81	0.81	0.81
	DNN	1.00	0.91	0.81	0.81	0.81	0.81
RMSE	MLR	2.99	3.47	3.23	3.26	4.10	3.53
	XGBoost	0.34	2.19	2.95	2.97	2.94	2.82
	DNN	0.40	2.15	2.94	2.96	2.90	2.80
MAE	MLR	2.25	2.34	1.93	1.97	2.73	2.16
	XGBoost	0.25	0.68	0.89	0.94	1.02	0.88
	DNN	0.31	0.70	0.96	0.99	1.06	0.95

XGBoost model was slightly larger than the one predicted by the DNN model, as shown in the one-day heat flux plots in Fig. 11 (b), (d), and (f). Compared with the DNN model, XGBoost had a relatively simple model structure, and more importantly, its training time was much shorter.

Therefore, XGBoost was selected, and its predicted heat flux was used as the predictor to guide the thermal loop schedule selection. A relatively large difference between the ML-predicted and FEM-calculated heat fluxes was observed when changing the thermal loop schedule from IL or

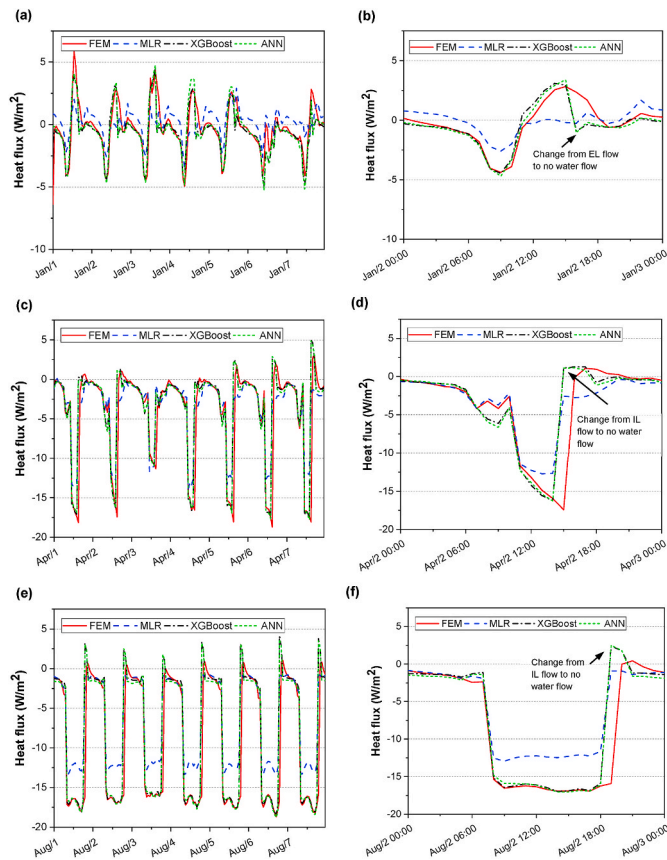


Fig. 11. Comparison of TEST-S1 heat flux predicted by the ML models for a typical week and a day in different seasons: (a) and (b) heating season week (January 1–7) and day (January 2), (c) and (d) transition season week (April 1–7) and day (April 2), and (e) and (f) cooling season week (August 1–7) and day (August 2).

EL to no water flow. This difference occurred mainly because the ML models were trained with constant water flows (CONST-S1–CONST-S3) in the thermal loops of TABE. Although ML models can efficiently predict the heat flux when the thermal loop schedule does not change frequently in a day, the models lack the ability to catch up the dynamics owing to changing the water flow from different thermal loop configurations in a short time period.

In addition, the annual heat flux was compared with the FEM calculated and the XGBoost predicted for TEST-S1, shown in Fig. 12(a). This comparison shows the heat flux behavior is similar to the representative weeks; for example, some of the heat fluxes were

overpredicted by XGBoost model during the cooling season, as shown in Fig. 11(e). All the heat fluxes plotted in Figs. 11 and 12 are of the south wall. All the remaining walls have heat flux behavior similar to the south wall and therefore are not plotted.

The effects of ground temperature uncertainty on the predicted heat flux were also studied, and the results are presented in Figs. 8(e) and Figure 12(b). The FEM results show that the uncertainty in the ground temperature caused a relatively small heat flux change, as shown in Fig. 8(e). The XGBoost predicted results were found to be similar to the FEM, as shown in Fig. 12(b). Additionally, this study found that the FEM and XGBoost results changed consistently as the ground temperature changed. This result indicates that the XGBoost model caught well the effects of ground temperature uncertainty.

Overall, the trained ML models, including the XGBoost and DNN models, performed well for the TABE heat flux prediction with respect to different thermal loop schedules and uncertainty of ground temperature. This study indicates that the trained ML models are capable of predicting TABE heat flux for different thermal loop schedules. This conclusion is important for similar applications because those applications only need to use data from constant thermal loop schedules to train the ML models. A relatively complex thermal loop schedule, such as the schedule OPT (see Table 5), should be used as the validation data to include potential system dynamics in the ML models. This study highlights the usefulness of ML in building energy management for active building envelopes, especially the water-based active building envelope.

3.3.2. Predictor-guided thermal loop schedule selection

The XGBoost-predicted heat fluxes were used as the inputs of the EnergyPlus model of the DOE prototype single-family residential building in Charleston to calculate the corresponding energy consumptions and costs. The calculated annual HVAC energy consumptions and costs of the test thermal loop schedules are presented in Table 7. The baseline energy consumption was obtained by directly running the prototype building in EnergyPlus. The energy costs were calculated by multiplying the obtained energy consumption of electricity and natural gas with their corresponding prices. The results show that TEST-S1 has the lowest energy consumption and cost, followed by TEST-S3, and TEST-S4 has the highest energy consumption and cost. The obtained energy consumptions and costs through the FEM-calculated and XGBoost-predicted heat fluxes are consistent with each other. The maximum annual energy cost difference between the obtained values is 4%, whereas FEM-calculated savings were 30%, and XGBoost-predicted savings were 26%. These results indicate that XGBoost-predicted heat flux can be used for thermal loop schedule selection.

The cooling energy consumption obtained by the XGBoost-predicted heat flux was constantly higher than the FEM-calculated heat flux because the XGBoost-predicted heat flux was higher when changing the thermal loop schedule from IL water flow to no water flow. However,

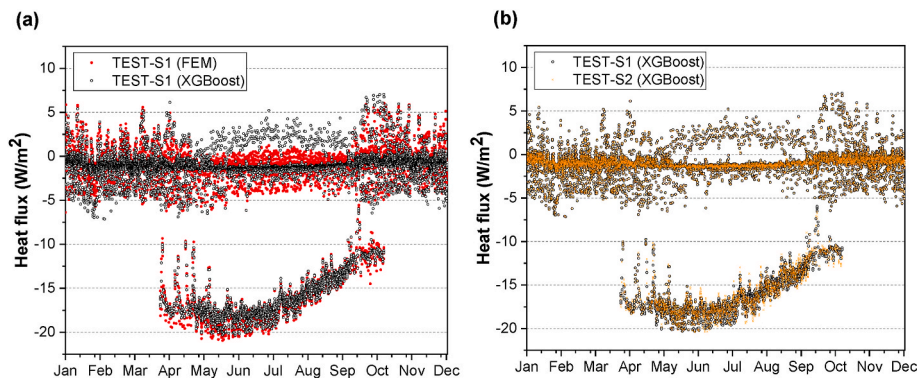


Fig. 12. Annual heat flux: (a) TEST-S1 FEM calculated vs. XGBoost predicted and (b) XGBoost predicted TEST-S1 vs. TEST-S2 (with considering ground temperature uncertainty).

Table 7
Annual HVAC energy consumptions and costs of the test water flow schedules.

	Electricity consumption*	Natural gas consumption	Electricity cost**	Natural gas cost***	Total cost savings
	MWh	MWh	\$	\$	%
Baseline	4.484	8.776	612	554	0
TEST-S1 (FEM)	2.084	8.417	284	531	30.0
TEST-S3 (FEM)	2.278	9.805	311	619	20.2
TEST-S4 (FEM)	2.473	9.848	337	621	17.7
TEST-S1 (XGBoost)	2.410	8.452	329	533	26.0
TEST-S3 (XGBoost)	2.563	9.741	350	615	17.3
TEST-S4 (XGBoost)	2.742	9.680	374	611	15.5

*The electricity consumption includes pump energy used to run the ground thermal loop. The pump has a power of 33 W **electricity price = 0.136 \$/kWh, ***natural gas price = 0.063 \$/kWh.

this consistently higher measurement will not influence a user's selection of a better thermal loop schedule for the building energy management when adopting TABE that uses a ground thermal loop.

Thermal loop schedules TEST-S3 and TEST-S4 led to a higher annual natural gas consumption. This higher consumption is mainly because the designed heating season schedules for these tests, HS2 and HS3, activated the IL during morning or night hours, as shown in Fig. 6(a). These schedules led to high heating requirements because the ground temperature (<20.5°C) is lower than the indoor setting temperature (22.2°C). Therefore, activating the EL during this time would be beneficial because the ground temperature is higher than the outdoor air temperature. This higher temperature is reflected in the natural gas consumption of the thermal loop schedule TEST-S1. However, the main purpose of the energy consumption and cost analysis was to show the effectiveness of applying the predicted heat flux in thermal loop schedule selection instead of optimizing the energy consumption and cost.

Another important aspect is the total computation time used for the annual building energy analysis for the baseline building installed TABE walls. For the ML predictor-guided analysis (XGBoost-predicted heat flux), the total computation time is less than 1 min for a specific thermal loop schedule. Thanks to the simple structure of XGBoost, the annual heat flux calculation for four TABE walls uses less than 20 s. Meanwhile, the energy consumption analysis in EnergyPlus uses less than 40 s. On the other hand, the FEM calculated case uses around 12 h to calculate the annual heat flux of four TABE walls. For the studied four test thermal loop schedules, the FEM calculation used a total of around 48 h while the XGBoost prediction used only around 4 min, being 720 times faster. The ML predictor enables the possibility of developing an optimization algorithm to find a suitable thermal loop schedule in future research. For example, the genetic based optimization such as particle swarm optimization involves sampling thousands of potential thermal loop schedules to find the potential optimum one. This becomes possible by using ML predicted heat flux for building installed TABE using ground energy source.

4. Conclusions and future research

In this study, a domain knowledge-informed, finite element-based ML framework was developed for the energy management of buildings installed with TABE that uses a ground thermal loop. Three ML models, MLR, XGBoost, and DNN, were employed to train and forecast the heat flux of TABE using the FEM simulated data sets under different thermal loop schedules. One of the ML models was selected based on three performance metrics and the predicted heat flux behavior. The predicted heat flux of different water flow schedules was used as the input of a DOE prototype building for building energy consumption estimations. Lastly, a water flow schedule was selected based on the energy consumption and its corresponding energy cost results. Based on the presented results, the following conclusions are drawn.

- The developed domain knowledge-informed, finite element-based ML framework can be applied to the energy management of buildings installed with TABE that uses a ground thermal loop. The energy consumption and cost obtained by the ML model are consistent with those obtained by the FEM for different thermal loop schedules.
- The XGBoost model is a good candidate for predicting the heat flux because it can reach good accuracy (e.g., R^2 value of 0.81) and is more efficient than the DNN model.
- The XGBoost-predicted heat flux of TABE that uses a ground thermal loop catches well the uncertainty of ground temperature. This fact has been shown by the consistency of the XGBoost-predicted heat flux with the FEM-calculated counterparts.
- The difference between the XGBoost-predicted and the FEM-calculated heat flux occurs mainly when the interior water flow changes to zero.
- The annual energy cost of the FEM-calculated savings is 30%, and the XGBoost-predicted savings are 26% with a difference of 4% indicating that the XGBoost-predicted heat flux can be applied to thermal loop schedule selection.
- The use of ML predictor-guided thermal loop schedule selection significantly reduced the annual building energy analysis time. For the baseline building installed with TABE, XGBoost reduced time from around 12 h (using FEM) to around 1 min. This enables the possibility of developing an optimization algorithm to find a suitable thermal loop schedule in the future.

Future research is needed to explore the following two aspects.

- The durability issue of TABE. As an active water-based building envelope, the application of TABE that uses a GL for building energy management involves pumps, pipes, fittings, and the TABE panels. Routine maintenance should ensure the normal operation of the system. Special attention should be paid to the durability of the TABE panel as it involves the anisotropic layers (e.g., thin Al foils) and water tubes. The difference in the thermal expansion coefficient of different materials may build internal stress in the TABE panel and potentially leads to problems like breakage of the thin Al foils. For these concerns, ORNL has launched a field evaluation for the TABE panels on a research experimental facility in Charleston, South Carolina, U.S. from early 2020. So far, we have not observed any failure of the TABE panels.
- The selection of the training and validation data sets. In this study, three constant schedules and an optimum schedule were used as the training and validation data sets. As stated in the results section (Section 3.3), the ML models lack the ability to catch up with the heat flux dynamics if the thermal loop configurations change rapidly. Future research is needed to understand how to build such dynamics into the training data set or the validation data set.

CRedit authorship contribution statement

Zhenglai Shen: Writing – original draft, Investigation, Formal

analysis, Data curation, Conceptualization. **Som Shrestha**: Writing – review & editing, Resources, Project administration, Investigation, Funding acquisition, Conceptualization. **Daniel Howard**: Writing – review & editing, Investigation, Data curation. **Tianli Feng**: Writing – review & editing, Methodology, Investigation, Formal analysis, Conceptualization. **Diana Hun**: Writing – review & editing, Supervision, Resources, Project administration. **Buxin She**: Writing – review & editing, Formal analysis, Data curation.

Declaration of competing interest

The authors declare the following financial interests/personal relationships which may be considered as potential competing interests: Som Shrestha reports financial support was provided by US Department of Energy. Som Shrestha has patent Thermally Anisotropic Composites for Thermal Management in Building Environments pending to UT-BATTELLE, LLC

Data availability

Data will be made available on request.

Acknowledgements

This research was supported by the DOE's Office of Energy Efficiency and Renewable Energy, Building Technologies Office under Contract No. DE-AC05-00OR22725 with UT-Battelle LLC and used resources at the Building Technologies and Research Integration Center, a DOE-EERE User Facility at Oak Ridge National Laboratory.

References

- [1] I. Hamilton, O. Rapf, Global Status Report for Buildings and Construction: towards a Zero-Emissions, Efficient and Resilient Buildings and Construction Sector, 2020. Paris, France, 2020, www.iea.org.
- [2] U.S. Energy Information Administration, Residential Energy Consumption Survey, 2009, 2012, <https://www.eia.gov/consumption/residential/data/2020/>.
- [3] U.S. Energy Information Administration, Commercial Buildings Energy Consumption Survey, 2003, 2008, https://www.eia.gov/consumption/commercial/data/2018/pdf/CBECS_2018_Building_Characteristics_Flipbook.pdf.
- [4] C. Harris, Opaque Envelopes: Pathway to Building Energy Efficiency and Demand Flexibility, 2021. <https://www.osti.gov/servlets/purl/1821413/%0Ahttps://www1.eere.energy.gov/buildings/pdfs/80170.pdf>.
- [5] S.B. Sadineni, S. Madala, R.F. Boehm, Passive building energy savings: a review of building envelope components, *Renew. Sustain. Energy Rev.* 15 (2011) 3617–3631, <https://doi.org/10.1016/j.rser.2011.07.014>.
- [6] Z. Tian, X. Zhang, X. Jin, X. Zhou, B. Si, X. Shi, Towards adoption of building energy simulation and optimization for passive building design: a survey and a review, *Energy Build.* 158 (2018) 1306–1316, <https://doi.org/10.1016/j.enbuild.2017.11.022>.
- [7] R. Baetens, B.P. Jelle, A. Gustavsen, Aerogel insulation for building applications: a state-of-the-art review, *Energy Build.* 43 (2011) 761–769, <https://doi.org/10.1016/j.enbuild.2010.12.012>.
- [8] K. Biswas, Development and validation of numerical models for evaluation of foam-vacuum insulation panel composite boards, including edge effects, *Energies* 11 (2018), <https://doi.org/10.3390/en11092228>.
- [9] R. Baetens, B.P. Jelle, J.V. Thue, M.J. Tenpierik, S. Grynning, S. Uvsløkk, A. Gustavsen, Vacuum insulation panels for building applications: a review and beyond, *Energy Build.* 42 (2010) 147–172, <https://doi.org/10.1016/j.enbuild.2009.09.005>.
- [10] N. Simões, M. Gonçalves, C. Serra, S. Resalati, Can vacuum insulation panels be cost-effective when applied in building façades? *Build. Environ.* 191 (2021) <https://doi.org/10.1016/j.buildenv.2021.107602>.
- [11] J.H. Kim, F.E. Boafso, S.M. Kim, J.T. Kim, Aging performance evaluation of vacuum insulation panel (VIP), *Case Stud. Constr. Mater.* 7 (2017) 329–335, <https://doi.org/10.1016/j.cscm.2017.09.003>.
- [12] D. Olsthoorn, F. Haghighat, A. Moreau, G. Lacroix, Abilities and limitations of thermal mass activation for thermal comfort, peak shifting and shaving: a review, *Build. Environ.* 118 (2017) 113–127, <https://doi.org/10.1016/j.buildenv.2017.03.029>.
- [13] Q. Al-Yasiri, M. Szabó, Incorporation of phase change materials into building envelope for thermal comfort and energy saving: a comprehensive analysis, *J. Build. Eng.* 36 (2021), <https://doi.org/10.1016/j.jobbe.2020.102122>.
- [14] P.K.S. Rathore, N.K. Gupta, D. Yadav, S.K. Shukla, S. Kaul, Thermal performance of the building envelope integrated with phase change material for thermal energy storage: an updated review, *Sustain. Cities Soc.* 79 (2022), 103690, <https://doi.org/10.1016/j.scs.2022.103690>.
- [15] Y. Luo, L. Zhang, M. Bozlar, Z. Liu, H. Guo, F. Meggers, Active building envelope systems toward renewable and sustainable energy, *Renew. Sustain. Energy Rev.* 104 (2019) 470–491, <https://doi.org/10.1016/j.rser.2019.01.005>.
- [16] M. Ibáñez-Puy, C. Martín-Gómez, M. Vidaurre-Arbizu, J.A. Sacristán-Fernández, Theoretical design of an active façade system with peltier cells, *Energy Proc.* 61 (2014) 700–703, <https://doi.org/10.1016/j.egypro.2014.11.946>.
- [17] X. Xu, S. Wang, J. Wang, F. Xiao, Active pipe-embedded structures in buildings for utilizing low-grade energy sources: a review, *Energy Build.* 42 (2010) 1567–1581, <https://doi.org/10.1016/j.enbuild.2010.05.002>.
- [18] Q. Zhu, X. Xu, J. Wang, F. Xiao, Development of dynamic simplified thermal models of active pipe-embedded building envelopes using genetic algorithm, *Int. J. Therm. Sci.* 76 (2014) 258–272, <https://doi.org/10.1016/j.ijthermalsci.2013.09.008>.
- [19] Z. Liu, L. Zhang, G. Gong, Y. Luo, F. Meng, Evaluation of a prototype active solar thermoelectric radiant wall system in winter conditions, *Appl. Therm. Eng.* 89 (2015) 36–43, <https://doi.org/10.1016/j.applthermaleng.2015.05.076>.
- [20] Z. Liu, L. Zhang, G. Gong, T. Han, Experimental evaluation of an active solar thermoelectric radiant wall system, *Energy Convers. Manag.* 94 (2015) 253–260, <https://doi.org/10.1016/j.enconman.2015.01.077>.
- [21] M. Dabbagh, M. Krarti, Evaluation of the performance for a dynamic insulation system suitable for switchable building envelope, *Energy Build.* 222 (2020), 110025, <https://doi.org/10.1016/j.enbuild.2020.110025>.
- [22] K. Biswas, S. Shrestha, D. Hun, J. Atchley, Thermally anisotropic Composites for improving the energy efficiency of building envelopes, *Energies* 12 (2019) 195–209, <https://doi.org/10.3390/en12193783>.
- [23] K. Biswas, S. Shrestha, D. Hun, J. Atchley, Thermally anisotropic Composites for heat redirection and thermal management in building envelopes, in: 2019 Therm. Perform. Exter. Envel. Whole. Build. XIV Int. Conf., Clearwater, Florida, 2019.
- [24] S. Shrestha, K. Biswas, D. Hun, J. Atchley, Thermally Anisotropic Composites for Thermal Management in Building Environments, 2020. <https://patents.google.com/patent/US20200326085A1/en>.
- [25] D. Howard, S. Shrestha, Z. Shen, T. Feng, Field evaluation and numerical study to determine the energy saving potential of thermally anisotropic building envelope, *Energy Build.* (2022) under review.
- [26] A. Fouquier, S. Robert, F. Suard, L. Stéphan, A. Jay, State of the art in building modelling and energy performances prediction: a review, *Renew. Sustain. Energy Rev.* 23 (2013) 272–288, <https://doi.org/10.1016/j.rser.2013.03.004>.
- [27] M.I. Jordan, T.M. Mitchell, Machine learning: trends, perspectives, and prospects, *Science* 80 (2015) 349.
- [28] Z. Wang, R.S. Srinivasan, A review of artificial intelligence based building energy use prediction: contrasting the capabilities of single and ensemble prediction models, *Renew. Sustain. Energy Rev.* 75 (2017) 796–808, <https://doi.org/10.1016/j.rser.2016.10.079>.
- [29] Y. Zhou, J. Wang, Y. Liu, R. Yan, Y. Ma, Incorporating deep learning of load predictions to enhance the optimal active energy management of combined cooling, heating and power system, *Energy* 233 (2021), 121134, <https://doi.org/10.1016/j.energy.2021.121134>.
- [30] Z. Wang, T. Hong, M.A. Piette, Building thermal load prediction through shallow machine learning and deep learning, *Appl. Energy* 263 (2020), 114683, <https://doi.org/10.1016/j.apenergy.2020.114683>.
- [31] L. Zhang, J. Wen, Y. Li, J. Chen, Y. Ye, Y. Fu, W. Livingood, A review of machine learning in building load prediction, *Appl. Energy* 285 (2021), 116452, <https://doi.org/10.1016/j.apenergy.2021.116452>.
- [32] C. Lu, S. Li, Z. Lu, Building energy prediction using artificial neural networks: a literature survey, *Energy Build.* 262 (2022), 111718, <https://doi.org/10.1016/j.enbuild.2021.111718>.
- [33] Y. Chen, M. Guo, Z. Chen, Z. Chen, Y. Ji, Physical energy and data-driven models in building energy prediction: a review, *Energy Rep.* 8 (2022) 2656–2671, <https://doi.org/10.1016/j.egy.2022.01.162>.
- [34] S. Fathi, R. Srinivasan, A. Fenner, S. Fathi, Machine learning applications in urban building energy performance forecasting: a systematic review, *Renew. Sustain. Energy Rev.* 133 (2020), 110287, <https://doi.org/10.1016/j.rser.2020.110287>.
- [35] A. Briga-Sá, D. Leitão, J. Boaventura-Cunha, F.F. Martins, Trombe wall thermal performance: data mining techniques for indoor temperatures and heat flux forecasting, *Energy Build.* 252 (2021), 111407, <https://doi.org/10.1016/j.enbuild.2021.111407>.
- [36] M. Martínez-Comesaña, L. Febrero-Garrido, E. Granada-Álvarez, J. Martínez-Torres, S. Martínez-Mariño, Heat loss coefficient estimation applied to existing buildings through machine learning models, *Appl. Sci.* 10 (2020) 1–18, <https://doi.org/10.3390/app10248968>.
- [37] F. Scarselli, A. Chung Tsoi, Universal approximation using feedforward neural networks: a survey of some existing methods, and some new results, *Neural Network.* 11 (1998) 15–37, [https://doi.org/10.1016/S0893-6080\(97\)00097-X](https://doi.org/10.1016/S0893-6080(97)00097-X).
- [38] O.I. Abiodun, A. Jantan, A.E. Omolara, K.V. Dada, N.A.E. Mohamed, H. Arshad, State-of-the-art in artificial neural network applications: a survey, *Heliyon* 4 (2018), e00938, <https://doi.org/10.1016/j.heliyon.2018.e00938>.
- [39] S.M.C. Magalhães, V.M.S. Leal, I.M. Horta, Modelling the relationship between heating energy use and indoor temperatures in residential buildings through Artificial Neural Networks considering occupant behavior, *Energy Build.* 151 (2017) 332–343, <https://doi.org/10.1016/j.enbuild.2017.06.076>.
- [40] M.W. Ahmad, M. Mourshef, Y. Rezgui, Trees vs Neurons: comparison between random forest and ANN for high-resolution prediction of building energy consumption, *Energy Build.* 147 (2017) 77–89, <https://doi.org/10.1016/j.enbuild.2017.04.038>.

- [41] D. Chauhan, J. Thakur, Data mining techniques for weather prediction: a review, *Int. J. Recent Innov. Trends Comput. Commun.* 2 (2014).
- [42] S. Ghimire, R.C. Deo, N. Raj, J. Mi, Deep solar radiation forecasting with convolutional neural network and long short-term memory network algorithms, *Appl. Energy* 253 (2019), 113541, <https://doi.org/10.1016/j.apenergy.2019.113541>.
- [43] L. Xing, J.D. Spitler, Prediction of undisturbed ground temperature using analytical and numerical modeling. Part I: model development and experimental validation, *Sci. Technol. Built Environ.* 23 (2017) 787–808, <https://doi.org/10.1080/23744731.2016.1258371>.
- [44] T. Chen, C. Guestrin, XGBoost: a scalable tree boosting system, in: *Proc. ACM SIGKDD Int. Conf. Knowl. Discov. Data Min.*, 2016, pp. 785–794, <https://doi.org/10.1145/2939672.2939785>.
- [45] A. Shrestha, A. Mahmood, Review of deep learning algorithms and architectures, *IEEE Access* 7 (2019) 53040–53065, <https://doi.org/10.1109/ACCESS.2019.2912200>.
- [46] C.C. Aggarwa, *Neural Networks and Deep Learning*, Springer International Publishing, 2018, <https://doi.org/10.1111/phor.12376>.
- [47] J. Bergstra, D. Yamins, D. Cox, Hyperopt: a Python library for optimizing the hyperparameters of machine learning algorithms, *Proc. 12th Python Sci. Conf.* (2013) 13–19, <https://doi.org/10.25080/majora-8b375195-003>.
- [48] T. Chai, R.R. Draxler, Root mean square error (RMSE) or mean absolute error (MAE)? -Arguments against avoiding RMSE in the literature, *Geosci. Model Dev. (GMD)* 7 (2014) 1247–1250, <https://doi.org/10.5194/gmd-7-1247-2014>.
- [49] U.S. Department of Energy, *Prototype Building Models*, 2018. <https://www.energycodes.gov/prototype-building-models>. (Accessed 25 October 2022).
- [50] J. Cai, J. Luo, S. Wang, S. Yang, Feature selection in machine learning: a new perspective, *Neurocomputing* 300 (2018) 70–79, <https://doi.org/10.1016/j.neucom.2017.11.077>.
- [51] F. Pedregosa, G. Varoquaux, A. Gramfort, B. Thirion, O. Grisel, M. Blondel, P. Prettenhofer, R. Weiss, V. Dubourg, J. Vanderplas, A. Passos, D. Cournapeau, M. Brucher, M. Perrot, E. Duchesnay, Scikit-learn: machine learning in Python, *J. Mach. Learn. Res.* 12 (2011) 2825–2830, <https://doi.org/10.1289/EHP4713>.